Front-End Design for Non-Invasive Electrical Resistance Tomography for Liquid Column

Yasmin Abdul Wahab[1], Ruzairi Abdul Rahim[2,3], Mohd Anwar Zawawi[1], Mohd Hafiz Fazalul Rahiman[4], Leow Pei Ling[3], Juliza Jamaluddin[5], Helen Goh[3], Suzanna Ridzuan Aw[6] and Herlina Abdul Rahim[3]
[1]*Faculty of Electrical and Electronic Engineering, Universiti Malaysia Pahang, 26600 Pekan, Pahang*
[2]*Faculty of Electrical and Electronic Engineering, Universiti Tun Hussein Onn, 86400 Batu Pahat, Johor*
[3]*Faculty of Electrical Engineering, Universiti Teknologi Malaysia, 81310 Skudai, Johor*
[4]*School of Mechatronic Engineering, Universiti Malaysia Perlis, 02600 Arau, Perlis*
[5] *Faculty of Science and Technology, Universiti Sains Islam Malaysia, 71800 Bandar Baru Nilai, Negeri Sembilan, Malaysia*
[6]*Faculty of Electrical & Automation Engineering Technology, TATiUC, 24000 Kemaman, Terengganu*
yasmin@ump.edu.my

***Abstract*—This paper explains the front-end design for non-invasive electrical resistance tomography. The electrical resistance tomography system presented in this paper uses high-frequency potential. In this design, the phase-shift demodulation (PSD) approach was eliminated and replaced by a peak detector circuit. The switching between transmitter/receiver and the transmitting channel was controlled by an analogue switch, MAX319 and demultiplexer, DG406, respectively. A microcontroller was applied to the data acquisition which eliminates the needs of a data acquisition system. Sensor readings of each receiver from each transmitter groups were tested experimentally, compared and analysed with simulation results. These experimental readings were compared with the sensors reading simulated from COMSOL Multiphysics software. As a result, the current values between 0-1mA from experiments was similar with the simulation results for all groups of transmitters. Thus, it can be concluded that the front-end design can be applied for the non-invasive ERT when high frequency is considered.**

***Index Terms*—Non-Invasive; ERT; High Frequency; Liquid-Solid.**

I. INTRODUCTION

A mixture such as liquid-liquid, liquid-solid and liquid–gas two-phase regime is the main concern in industrial applications. The industry applications involving mixtures, for example, are bubble column, fluidized bed reactor, stirred tank reactor and vertical or horizontal vessel. Visualization at an early stage of the mixtures in an industrial application may promise a good performance and prevents any unwanted condition during process time. One of the methods that can do this preceding visualization is called Electrical Resistance Tomography (ERT). There are many examples of ERT system that have been studied focusing on imaging technique of the liquid column. However, only a few researchers have considered the ERT with non-invasive sensing technique [1]–[7]. Also, the presented results still have an obvious limitation which is the needs of a complex circuits design. The work in this paper has thus been deliberately developing a new non-invasive ERT system that can produce a better performance analysis for the multiphase mixtures.

Besides, the conventional technique of ERT is applied invasively to the pipeline. This technique will cause the electrodes of ERT to have a direct contact with the conductive liquid inside the vessel. The direct contact between the electrodes and the conductive liquid such as electrolyte will cause an oxidation to the electrode. This process occurs due to the conversion of the chemical reaction and electrical energy which is known as electrochemical erosion effect. Consequently, this situation will lead to corrosion of the electrodes hence reduce the sensor lifespan [5], [6]. Thus, inconsistency in measurement with unpredictable error will be produced. Due to this limitation, the use of invasive ERT system in the industrial application is limited.

This problem can be solved by employing the non-invasive technique of ERT system. A placement of the electrode on the periphery of the pipe wall can avoid the electrode from being affected by the electrochemical process. Without direct contact, the sensor lifespan can be improved as well as increase its capability to be implemented in the industrial application.

Moreover, most of the presented works for ECT and ERT have preferred to develop the system with frequency in kHz. At this point, a phase sensitive demodulation (PSD) method using sophisticated circuit design also needs to be developed in conjunction with the ECT or ERT system development for measuring the internal permittivity or internal conductivity like in Ref. [8]–[15]. Thus, in this work, we prove that by developing the non-invasive ERT system with high-frequency level, PSD technique will not be required. The utilization of high-frequency level enables the system to detect the internal information of conductivity of the medium of interest.

II. NON-INVASIVE PRINCIPLES

Electrical resistance tomography used to reconstruct the image based on resistance distribution or conductivity distribution of the medium interest. In process tomography applications, the resistance is measured by exciting voltage (or current) and detecting current (or voltage) via sensors mounted on the circumference of pipe walls [16]. Electrical tomography sensing field applies the knowledge of the electromagnetic field theory. Equation (1) shows the quasi-static electric field of non-invasive ERT.

The Γ_i and Γ_j represent the spatial locations of n electrodes; i and j are the indexes of excitation and detection electrodes respectively, V_o is the applied voltage to the system, and n indicates the outward unit normal vector. It is clearly seen that the non-invasive ERT is influenced by the conductivity, σ and

$$\begin{cases} \nabla.(\sigma(x,y)+j\omega\varepsilon(x,y))\nabla V(x,y)=0 & (x,y)\subseteq\Omega \\ V_i(x,y)=V_0 & (x,y)\subseteq\Gamma_i \\ V_j(x,y)=0 & (x,y)\subseteq\Gamma_j \\ \dfrac{dV(x,y)}{dn}=0 & (x,y)\subseteq\Gamma_k,(k\neq i,j) \end{cases} \quad (1)$$

relative permittivity, ε which due to the conductive medium, and insulating pipe implemented. The ω represents the angular frequency of the excitation AC source. The main reason why electric quasi-static (EQS) plays important role in the sensing field is due to the need of current flow through the two different mediums, which are the insulating pipe and the conductive medium.

Unfortunately, since the insulating pipe was implemented as a part of the sensing field for the non-invasive ERT system, the coupling capacitance of the insulating pipe is also generally considered for the sensing field, as in Figure 1. The coupling capacitance refers to the capacitance between the electrode mounted on the insulating pipe wall and the conductive liquid. Thus, it has two coupling capacitances for one pair of the measurement electrodes. It is very different if compared to the conventional ERT system, which only considers the resistance between each pair of the measurement electrodes.

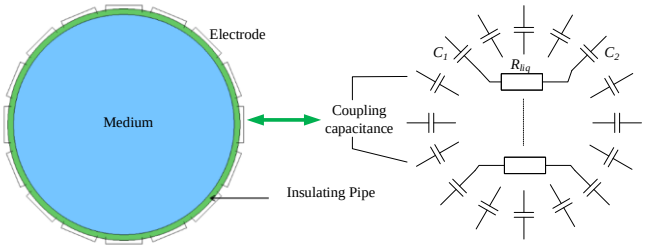

Figure 1: Non-Invasive ERT and its equivalent circuit

In that case, the non-invasive ERT system assumed to have total impedance, Z_{total} of resistance in series with the coupling capacitances as in Equation (2).

$$Z_{total}=R_{liq}-j\frac{1}{2\pi f\left(\dfrac{C_1C_2}{C_1+C_2}\right)} \quad (2)$$

However, according to Ohm's law, Equation (2) can be reduced to the resistance part only at a high-frequency region. The Ri,j, Vo and Ii,j in Equation (3) refers to the value of the resistance, voltage and current for every pair of the electrodes, respectively. The value of the resistance will be used later for the image reconstruction part to relate with the conductivity distribution of the medium of interest. The current value, Ii,j was assumed to be as the conduction current and hence it was only based on the electrical conductivity, σ and electric field, E between the i-j.

$$Z_{total}=R_{i,j}=real\frac{V_0}{I_{i,j}} \quad (3)$$

Thus, the conductance between *i-j*, $G_{i,j}$ is inverse proportional to resistance and hence was simplified as Equation (4). *s* is the surface of the detection electrode, and *ds* is the differential area of electrode's surface.

$$G_{i,j}=\frac{1}{R_{i,j}}=\frac{I_{i,j}}{V_0}=\frac{1}{V_0}\oint_s\sigma.\mathrm{E}ds \quad (4)$$

III. Sensor Design

The sixteen metal electrodes, each with 200 mm length and 16 mm width of non-invasive ERT, were made of flexible printed circuit boards because they could be easily bendable. The sensor designed is illustrated in Figure 2. The area of electrode other than the sensing area was shielded by connecting it to the ground to avoid the surrounding noise. A sensor jig was designed to stick and hold each of the sixteen sensors independently as illustrated in Figure-3. The design of the sensor jig was flexible in ensuring that the jig can also be applied to other pipes if necessary. It means that the sensor jig for each the sixteen channels can be unscrewed independently. Simultaneously, a ring holder with two screw locks on the upper and lower sides of the pipe was also designed to hold the sensor jigs. The insulating pipe was an acrylic tube with an outer diameter 100 mm, thickness 2 mm and height 500 mm.

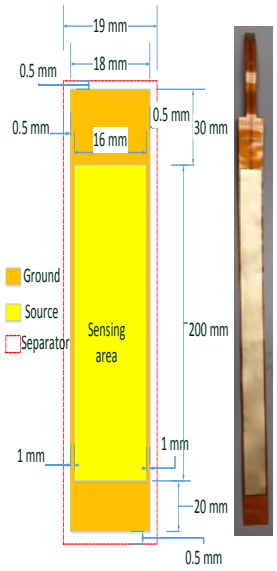

Figure 2: Non-invasive sensor design

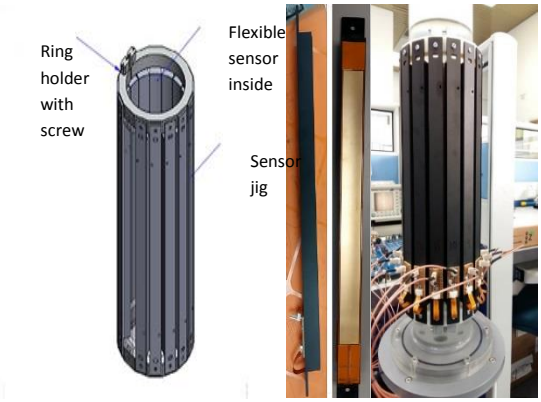

Figure 3: From left: A ring holder with sensor jigs, example of sensor jig from side and inner view, sensor jig attached to vertical pipe

IV. ELECTRONIC MEASUREMENT DESIGN

As shown in Figure 4, each of the sixteen channels was switched as a transmitter or receiver by using an analogue switch integrated circuit, MAX319. The circuit was controlled by microcontroller dsPIC30F6010A. There were two main parts of the designed circuits: signal generator circuit and signal conditioning circuit.

Firstly, a sinusoidal voltage signal was generated by the signal generator circuit. The direct digital synthesis (DDS) integrated component was chosen to produce the sinusoidal signal at frequency 2 MHz. It was programmed by the microcontroller PIC18F4580. Then, the signal was switched according to the transmitter channel by using demultiplexer, DG406B. The signal from the selected transmitter channel then amplified up to 10 Vpp by using amplifier circuit and applied to the transmitter.

Secondly, in the signal conditioning circuits; the current signal at the receiver was fed into a current to voltage converter amplifier circuit and filtered using a low pass filter. As a result, the converted signal would be in the range of 2 MHz and eliminated for all the possible noise. Since the high frequency has been applied, it was a challenge to choose the best and simplest technique in converting the sinusoidal signal into the direct current (DC) signal so that it could easily be used for reconstructing into an image. In short, the peak detector circuit was designed to convert the alternate current (AC) to DC signal.

The DC signal was sampled by dsPIC30F6010A so that it can be applied for getting the tomogram in the tomography image reconstruction. The overall durations for both the hardware and the software were calculated using start/stop watch timer in MATLAB. The hardware duration was around 60 ms and the software duration was around 190 ms. Thus, the total duration of the working system was 250 ms and this gave the system speed around 4 frames per second.

A. Signal Generator Circuit

There were three parts in the signal generator circuit: the DDS, demultiplexer, and amplifier circuits.

The integrated circuit AD9833 was chosen for producing the sinusoidal waveform at 2 MHz frequency. Also, the schematic diagram of the AD9833 to link with the PIC18F4580 was illustrated in Figure 5. The active low control input, FSYC pin was connected to the chip select, CS/RE2 pin. The serial clock input, SCLK pin was attached to the serial clock, SCK/RC3 pin. The serial data input, SDATA pin was linked to the serial data out, SDO/RC5 pin at PIC18F4580. Also, the MCLK pin from AD9833 was connected to the oscillator pin RA6 of PIC18F4580. The 51 Ω resistors at each of the SPI pin were applied to avoid the glitch signal. Figure 6 shows the real output of AD9833 measured by the oscilloscope. The sinewave was at 2 MHz with the amplitude around 460 mVpp. Thus, the amplifier circuit was needed to amplify up to 10 Vpp.

The demultiplexer was used as a switch for linking between the sinusoidal waveform from AD9833 to the amplifier circuit when the channel was acting as the transmitter. The DG406B was chosen as the demultiplexer because it allowed a current up to 30 mA for every terminal with a fast transition time within 115 ns. The DG406B is a high performance sixteen channels CMOS analogue multiplexer. It allows the current to conduct in both directions for each of the active channels. The enable (EN) pin is to reset the chip, either it functions as the multiplexer or demultiplexer to all the stacking several devices. Besides, the switching of each channel was controlled digitally by setting the EN pin to logic '1' and the control inputs as the truth table in the datasheet.

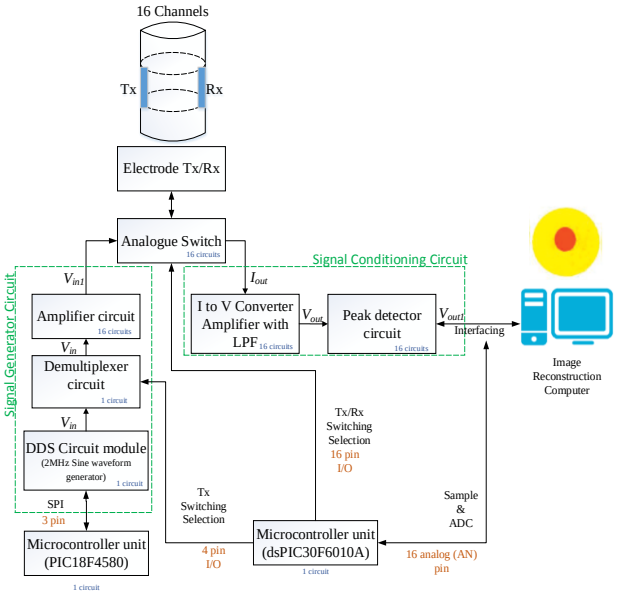

Figure 4: Experimental setup for non-invasive ERT system

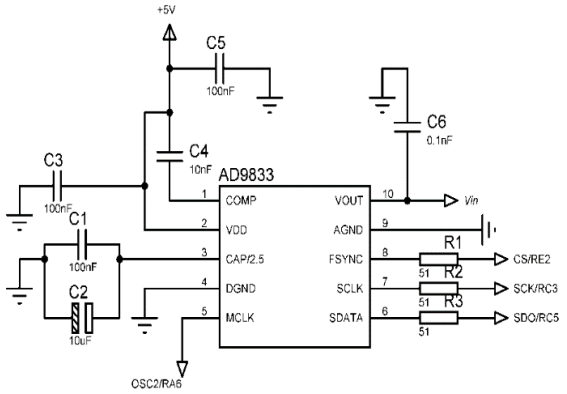

Figure 5: Connection pin of AD9833

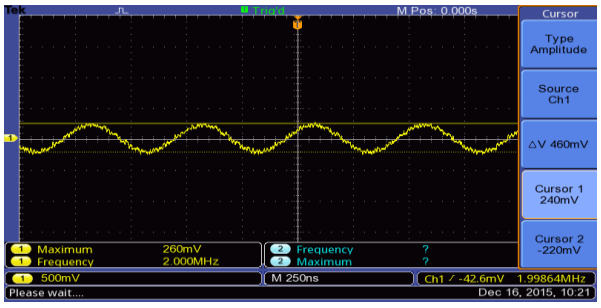

Figure 6: Output of 2 MHz sinusoidal waveform from AD9833

The LT1226, a low noise and high-speed operational amplifier, was selected to amplify the output signal from AD9833 up to 10Vpp. The 400 V/us slew rate, 1 GHz gain-bandwidth product and fast rise, fall and transition times made the LT1226 suitable to be used. Figure 7 illustrates the schematic diagram of the amplifier circuit. The inverting amplifier approach was applied and the gain was measured based on Equation (5). Since the output from AD9833 had

around 460mV, thus by implementing gain of 22 it gave the output of sine waveform at transmitter around 10 Vpp.

$$V_{in1} = -\frac{R5}{R4} \times V_{tx1} = -\frac{22K}{1K} \times 460\,m = 10.12\ \text{Vpp} \approx 10\ \text{Vpp} \quad (5)$$

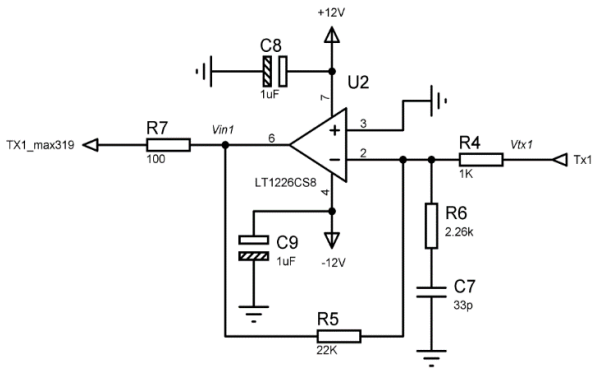

Figure 7: Schematic diagram of amplifier circuit

The components R6, C7, and R7 were utilized to ensure that the signal through the circuit could be maintained at the desired value when connected to the sensor. Figure 8 shows the signal from the LT1226 circuit after amplified. The measured sinusoidal waveform was almost 10 Vpp at 2 MHz.

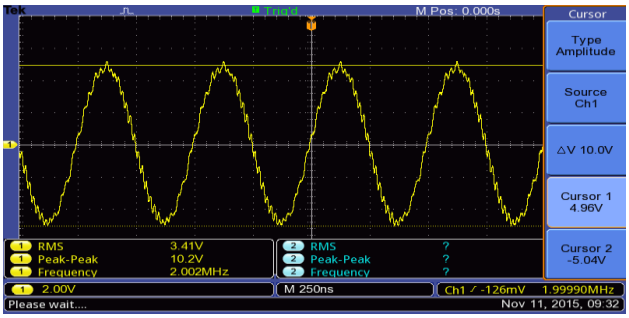

Figure 8: Signal of amplifier circuit

B. *Signal Conditioning Circuit*

The current signal that had been received at the detected electrode must be changed into a voltage level for easier next steps of signal processing before interfacing with the computer. Hence, the current to voltage, I-V converter amplifier was employed in the electronic measurement circuit.

The high speed and very high slew rate of the operational amplifier, LT1360 was chosen to perform the I-V converter amplifier. Figure 9 illustrates the schematic diagram of I-V converter amplifier circuit. Equation (6) shows the current to voltage conversion [22]. For instance, when the output current at receiver was 1.8 mA, then, the converted output voltage would be around 4 Vpp.

The resistor of 2.26 kΩ was chosen to ensure that the amplitude of the converted voltage was not exceeded 5 V to simplify the next steps of designing and interfacing the circuit with the microcontroller unit. Each of the electrodes would give different values in current and these resulted in the different values of the converted voltage levels. Also, to maintain the system at frequency 2 MHz, the parasitic capacitor, C10 was added to the circuit to have a combination with a resistor, R9 to perform as a low pass filter to stabilize the circuit [23]. The value of the capacitor was calculated using Equation (7). The resistor, R8 was connected to the

$$V_{out} = -I_{out} \times R9$$
$$V_{out} = -1.8mA \times 2.26K = 4.068V_{pp} \approx 4V_{pp} \quad (6)$$

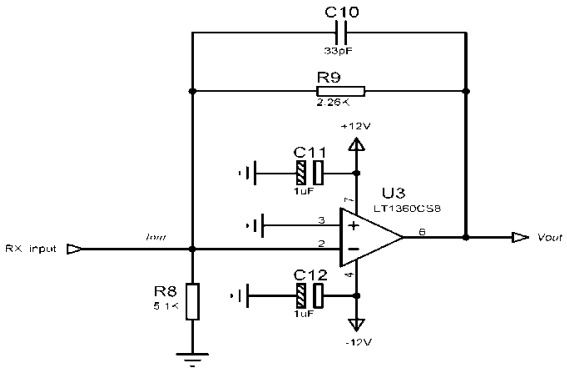

Figure 9: Schematic diagram of I-V amplifier circuit

inverting input of the operational amplifier to the ground was to maintain the current flow from the pin of entry.

$$C10 = \frac{1}{2\pi \times R5 \times f_{cut-off}} = \frac{1}{2\pi \times 2.26K \times 2.1M} = 33.53pF \approx 33pF \quad (7)$$

Figure 10 shows the example of I-V converter amplifier output. The output was maintained at frequency 2 MHz.

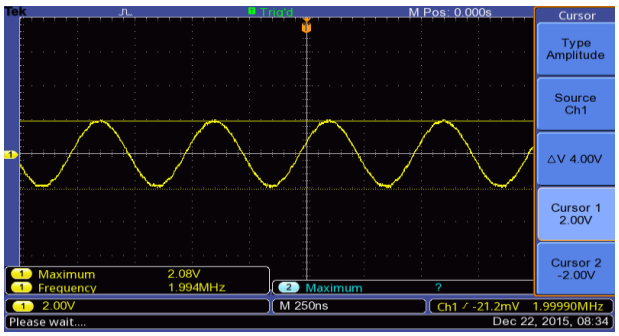

Figure 10: Output of I-V converter amplifier

Figure 11 shows the peak detector circuit applied in the electronic circuit measurement. The peak detector circuit was to output the peak value of the input AC signal. It was constructed with a dual and quad high-speed operational amplifier, LT1364 and a polyester capacitor, C13 to hold the peak value of the applied AC voltage from the previous circuit. When the input voltage was rising, the capacitor would then be charged to a new peak value. Meanwhile, when the AC signal was falling, the Schottky diodes (D1 and D2) would prevent the capacitor from discharging.

Furthermore, the high frequency (2 MHz) system needed a fast switching action so the Schottky diode, BAT81 that has a low forward voltage drop, could fulfil this requirement. In term of time consumption, a large value of capacitor will reduce the processing time to achieve the steady state signal and vice versa. The resistor R10 was engaged to prevent the current leakage through the entire circuit so that the output can be maintained at the dc value. Also, the second stage of operational amplifier was only used as a buffer. The example signal of peak value from the peak circuit is shown in Figure 12. The yellow line is the AC signal from the previous circuit, and the blue line is the peak signal. Later, the DC signal of

the peak detector circuit could be easily applied for the interfacing part.

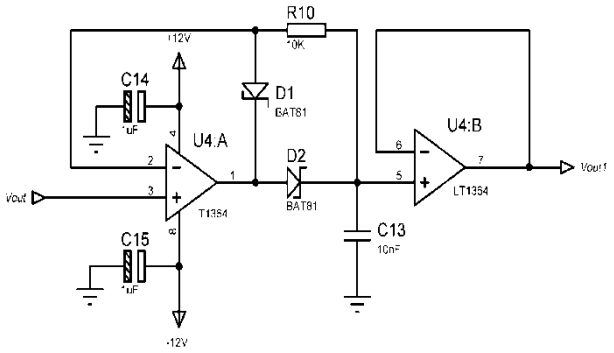

Figure 11: Schematic diagram of peak detector circuit

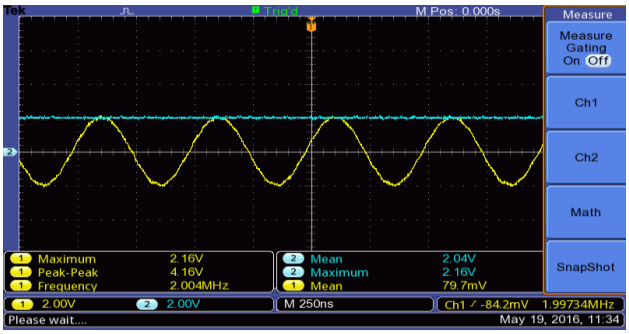

Figure 12: Example signal of peak value from AC signal

V. EXPERIMENTAL VERIFICATION

The experimental sensors reading of sixteen electrodes at the full conductive water (σ =7.3x10^{-3} S/m which measured using conductor meter) were compared and analysed with the simulation results from COMSOL Multiphysics. The data was divided into two groups; experiment group and simulation group. For each of the transmitter, all receivers were set as one group each. Thus, there were sixteen groups of each experiment and simulation. 240 measurement data of 16 times incentive determined from the simulation and experiment is illustrated in Figure 13. The voltage readings obtained from the experiment converted into current values for comparison with the simulation values. Under the comparison, it can be highlighted that the U-shape pattern for each transmitter groups remained significantly. It is believed that the fluctuation which occurred mainly at the adjacent electrodes in Figure 13(b) was due to the fringe effect, non-symmetrical sensors position and a slightly different of the real conductivity of the materials applied. Even the data from the online measurement was not symmetrical distribute as well as the simulation data; it still can be accepted because the range is between 0-1mA.

Besides, Figure 14 shows the example of tomogram obtained using an online system where the solid can be identified directly when it placed inside the pipe. The solid rod with 22 mm in diameter was placed in the pipe to test the capability of the electronic measurement design for reconstructing the image for the non-invasive ERT system at 2 MHz frequency. The position of tomogram was similar to the real position of the solid rod.

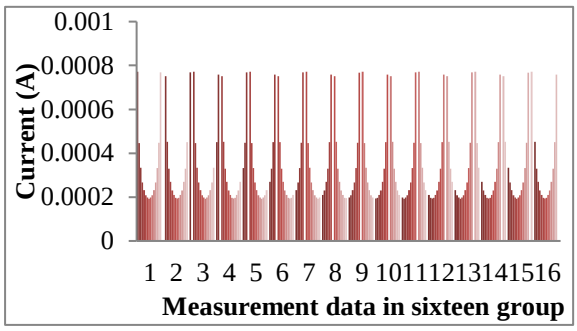

(a)

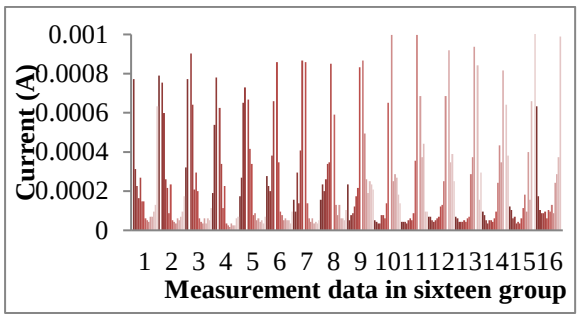

(b)

Figure 13: Collection of 240 measurement data of 16 times incentive non-invasive ERT system at homogenous field ; (a) simulation versus (b) experiment

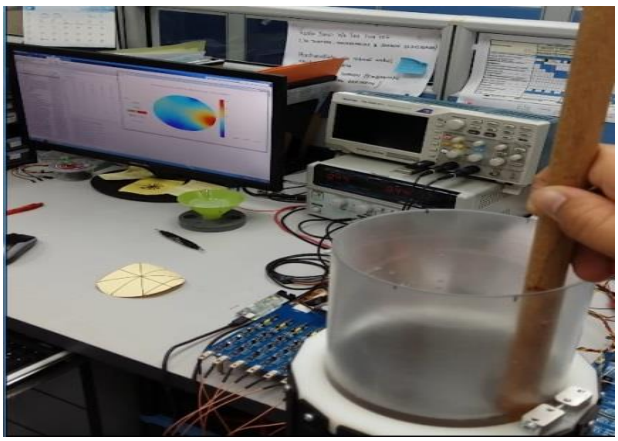

Figure 14: Example tomogram obtained in online system

VI. CONCLUSION

The front-end design of non-invasive ERT has been discussed. The presented study shows the electronic measurement design using high frequency (2 MHz) was able to be applied to the non-invasive ERT system. The assumption made allows the system based on the real part at high frequency. The simplicity of the circuit design with the development of peak detector circuit in the signal conditioning circuit was proven to reduce the complicity of phase shift demodulation technique. Besides, the flexible design of the sensors offered easy replacement of the sensors during troubleshooting process. Also, the analysis proved the verification of the experimental and simulation sensors reading. Lastly, the system was also able to reconstruct the two-phase regime of solid-liquid in the vertical column.

ACKNOWLEDGMENT

The authors thanks the Universiti Malaysia Pahang (RDU170368) for the support of this project.

REFERENCES

[1] Z. Cao, L. Xu, C. Xu, and H. Wang. "Electrical Resistance Tomography (ERT) by using An ECT Sensor". *In IEEE International Conference on Imaging Systems and Techniques*. pp. 63–66, 2010.

[2] B. L. Wang, Z. Y. Huang, H. F. Ji, and H. Q. Li. "Towards Capacitively Coupled Electrical Resistance Tomography". *In 6th World Congress on Industrial Process Tomography*. pp. 1574–1577, 2010.

[3] B. Wang, Y. Hu, H. Ji, Z. Huang, and H. Li. "A Novel Electrical Resistance Tomography System Based on C4D Technique". *In IEEE International Instrumentation and Measurement Technology Conference*. pp. 1929–1932, 1932.

[4] Y. Li and M. Soleimani "Imaging Conductive Materials with High Frequency Electrical Capacitance Tomography". *Measurement*. 46(9). pp. 3355–3361, 2013.

[5] B. Wang, Y. Hu, H. Ji, Z. Huang, and H. Li. "A Novel Electrical Resistance Tomography System Based on C4D Technique Technique". *IEEE Transactions on Instrumentation and Measurement*. 62(5). pp. 1017–1024, 2013.

[6] B. Wang, W. Zhang, Z. Huang, H. Ji, and H. Li, "Modeling and Optimal Design of Sensor for Capacitively Coupled Electrical Resistance Tomography System". *Flow Measurement and Instrumentation*. 31. pp. 3–9, 2013.

[7] B. Wang, W. Tan, Z. Huang, H. Ji, and H. Li. "Image Reconstruction Algorithm for Capacitively Coupled Electrical Resistance Tomography", *Flow Measurement and Instrumentation*. 40. pp. 216–222, 2014

[8] B. Wang, Z. Gui, W. Tan, Z. Huang, H. Ji, and H. Li, "A new dual-modality ECT/ERT technique based on C4D principle". *In IEEE International Conference on Instrumentation and Measurement Technology*. pp. 2061–2065, 2015.

[9] X. Ren and S. Liu. "Experimental study of phase sensitive detection technique in ect system". *In International Conference on Machine Learning and Cybernetics*.121–125, 2014

[10] B. Wang, Y. Hu, H. Ji, Z. Huang, and H. Li., "A Novel Electrical Resistance Tomography System Based on C4D Technique". *IEEE Transactions on Instrumentation and Measurement*. 62(5). pp. 1017–1024, 2013.

[11] D. Chen, W. Yang, S. Member, and M. Pan. ," Design of Impedance Measuring Circuits Based on Phase-Sensitive Demodulation Technique", *IEEE Transactions on Instrumentation and Measurement*. 60 (4). pp. 1276–1282, 2011.

[12] W. Yang. "Teaching phase-sensitive demodulation for signal conditioning to undergraduate students". *American Journal of Physics*. 78(9). pp. 909–915, 2010.

[13] X. Zhang and H. Wang, "Digital phase-sensitive demodulation in electrical capacitance tomography system". *In World Congress on Intelligent Control and Automation*. 2, pp. 6730–6733, 2008.

[14] W. Q. Yang, "Advance in AC-based capacitance tomography system". *In World Congress in Industrial Process Tomography*. pp. 557–564, 2011.

[15] W. Q. Yang. "Hardware design of electrical capacitance tomography systems". *Measurement Science and Technology*. 7. pp. 225–232, 1996.

[16] S. Hosseini, D. Patel, F. Ein-Mozaffari, and M. Mehrvar. "Study of Solid–Liquid Mixing in Agitated Tanks through Electrical Resistance Tomography: *Chemical Engineering Science.* 65(4), pp. 1374–1384, 2010.

[17] J. William H.Hayt and John A. Buck. *Engineering Electromagnetics*, 7th. Ed. Mc Graw Hill. New York. pp. 122., 2006.

[18] C. Kuo-Sheng, D. Isaacson, J. C. Newell, and D. G. Gisser. "Electrode Models for Electric Current Computed". *IEEE Transactions on Biomedical Engineering*. 36 (9). pp. 918–924, 1989.

[19] F. T. Ulaby, E. Michielssen, and U. Ravaioli. *Fundamentals of Applied Electromagnetics*, 6th Ed. Pearson. United State of America. pp. 196, 2010.

[20] F. T. Ulaby, E. Michielssen, and U. Ravaioli. *Displacement Current. In Fundamentals of applied electromagnetics*, 6th Ed. Pearson. United State of America. pp. 299–300, 2010.

[21] L. Riordan. 2010. An-1070 application note.

[22] R. L. Boylestad and L. Nashelsky. *Op-Amp Applications. In Electronic Devices and Circuit Theory*. 9th. Ed. Pearson. United State of America. pp. 640, 2006.

[23] K. S. Chan. "Real Time Image Reconstruction for Fan Beam Optical Tomography System". Master Thesis. Universiti Teknologi Malaysia, Skudai, Malaysia, 2002.